Dislocations and vacancies in two-dimensional mixed crystals of spheres and dimers

Sharon J. Gerbode,[1,*] Desmond C. Ong,[1] Chekesha M. Liddell,[2] and Itai Cohen[1]
[1]*Department of Physics, Cornell University, Ithaca, New York 14853, USA*
[2]*Materials Science and Engineering, Cornell University, Ithaca, New York 14853, USA*
(Received 7 August 2010; published 15 October 2010)

In colloidal crystals of spheres, dislocation motion is unrestricted. On the other hand, recent studies of relaxation in crystals of colloidal dimer particles have demonstrated that the dislocation dynamics in such crystals are reminiscent of glassy systems. The observed glassy dynamics arise as a result of dislocation cages formed by certain dimer orientations. In the current study, we use experiments and simulations to investigate the transition that arises when a pure sphere crystal is doped with an increasing concentration of dimers. Specifically, we focus on both dislocation caging and vacancy motion. Interestingly, we find that any nonzero fraction of dimers introduces finite dislocation cages, suggesting that glassy dynamics are present for any mixed crystal. However, we have also identified a vacancy-mediated uncaging mechanism for releasing dislocations from their cages. This mechanism is dependent on vacancy diffusion, which slows by orders of magnitude as the dimer concentration is increased. We propose that in mixed crystals with low dimer concentrations vacancy diffusion is fast enough to uncage dislocations and delay the onset of glassy dislocation dynamics.

DOI: 10.1103/PhysRevE.82.041404 PACS number(s): 82.70.Dd, 64.70.pv, 61.72.Ff, 61.72.jd

I. INTRODUCTION

Glassy dynamics are typically attributed to disordered systems ranging from jammed granular packs [1–3] to disordered spherical or anisotropic colloidal [4–8] and molecular [9–13] systems. Recent studies of defects within two-dimensional (2D) crystals of colloidal dimer particles have revealed that the introduction of particle anisotropy can also cause glassy relaxation within an ordered crystalline system [14]. Colloidal dimers consisting of two connected spherical lobes can fit into the same close-packed crystals that are formed by free spheres, with each lobe occupying a spherical crystal lattice position. This similarity implies that the study of colloidal dimers can isolate how a small anisotropic perturbation to the spherical particle shape can lead to new defect phenomena within a crystal.

Wojciechowski *et al.* were the first to study crystals of hard Brownian dimers. Their numerical simulations demonstrated that the ground state for 2D crystals of such particles is highly degenerate in the configurations of particle orientations [15,16]. In this "degenerate crystal" ground state, the dimer lobes occupy triangular lattice sites, but the particle orientations are not aligned in any periodic pattern. Instead, the particles are randomly oriented among the three underlying lattice directions.

The first experimental studies of degenerate crystals of dimers demonstrated that certain dimer orientations restrict the motion of dislocations within the crystal [17,18]. Further studies of mechanically perturbed degenerate crystals have revealed that dislocations are caged by particles in these glide-blocking orientations. Dislocation motion beyond such particles has been experimentally observed to occur through multidefect mechanisms that allow the defects to hop between cages [14]. This slow cage hopping is reminiscent of the motion of particles within a colloidal glass [5] and invites the question of how this glassy state is approached from the usual state of free dislocation motion in 2D crystals of spheres.

In the current study, we investigate the geometric restrictions to dislocation glide in mixed crystals composed of both spheres and dimers. Using numerical simulations we show that as the fraction of dimers in a mixed crystal is increased, the peak dislocation cage size decreases smoothly from infinity for pure sphere crystals down to several lattice constants (LC) in pure dimer crystals. This smooth scaling of the cage size suggests that glassy dislocation caging would be present for any nonzero dimer fraction. However, experimental observations of mixed crystals with small dimer concentrations reveal a vacancy-mediated dislocation uncaging mechanism where mobile vacancies can allow dislocations to climb and circumvent obstacles. This mechanism is enhanced by vacancy diffusion, which we observe to slow dramatically with increasing dimer concentration. Nevertheless, at low dimer concentrations, it may be rapid enough to alleviate glassy behavior.

II. EXPERIMENTAL SYSTEM AND NUMERICAL SIMULATION DETAILS

The experimental system has been described in detail elsewhere [14]. Briefly, sterically stabilized fluorescent silica dimer shells with lobe diameter $d \approx 1.3$ μm and lobe separation $l \approx 1.4$ μm are suspended in an index-matching aqueous solution of dimethylsulfoxide. The dimer shell particle synthesis protocol is described in [17]. Also included in the suspension are 1.3 μm diameter silica spheres (Sekisui Micropearl Spacers, Dana Enterprises International, CA). The suspension of dimers and spheres is confined in a wedge-shaped cell constructed from two bonded glass coverslips, as

*Present address: School of Engineering and Applied Sciences, Harvard University, Cambridge, MA 02138, USA. sgerbode@seas.harvard.edu

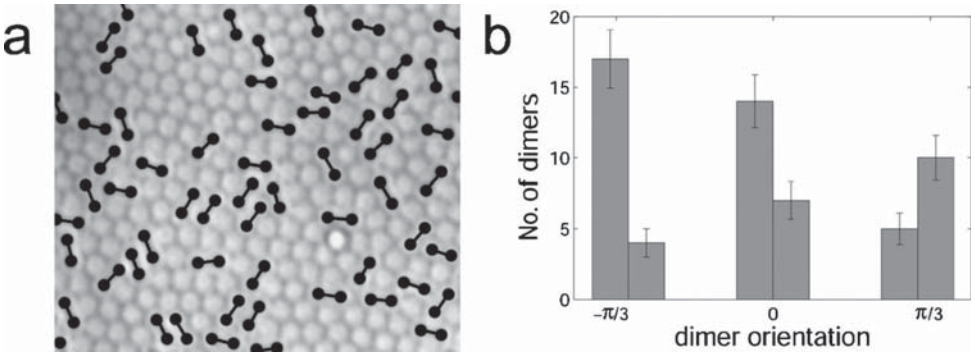

FIG. 1. (a) Optical microscope image of a mixed sphere and dimer crystal with ϕ_d=0.4. Dumbbells are overlaid on top of the dimers for clarity. The bright white sphere is an intruder particle. (b) Distribution of dimer orientations within the grain. Error bars are derived from counting statistics.

described in the Appendix. The particles are viewed in the "monolayer" region of the cell where the gap between the two coverslips only accommodates a single layer of particles lying flat. The density mismatch (~0.5 g/ml) between the shells and the fluid is exploited to sediment the particles into the monolayer region and to set the lobe area fraction to ~0.8, where the dimer shells and the spherical particles assemble into a crystalline phase [19].

The dimer particle synthesis produces samples with a small fraction of misshapen "mutant" dimer particles that have more than two lobes or are otherwise not dimer shaped. These mutant particles inhibit crystallization of mixtures of spheres and dimers. In order to form large mixed crystal grains, we first combine dimer and sphere suspensions and allow them to self-assemble into dense polycrystalline mixtures. To achieve complete crystallization into large mixed crystal grains, we use an optically manipulated spherical "intruder" particle to push out mutant particles and add true dimers to a crystal grain that is initially composed of mostly spheres. The intruder particles are 1.3-μm-diameter spheres composed of sterically stabilized silica-coated polystyrene [14]. The index mismatch between the intruder particles and the suspending fluid allows an optical trap to exert a force on the intruder particles with negligible effects on the silica dimer shells and spheres. Dimer particles are added to the mixed crystal grain until reaching a set dimer concentration ϕ_d, defined as the number of dimer lobes divided by the total number of lattice sites in the crystal grain. An example of one mixed crystal grain prepared using this procedure is shown in Fig. 1(a). While such mixed crystal grains are not fully self-assembled, the dimers are nevertheless oriented with approximately equal probability among the three lattice directions, as can be seen in the distribution of dimer orientations shown in Fig. 1(b).

This manual procedure for mixed crystal grain assembly is very slow, typically taking 1 week for each grain. Once such a grain is created, the distribution of dislocation cage sizes can be computed by counting how far a dislocation with any of the three possible Burgers vectors could glide from each starting lattice position. While in principle it would be possible to collect sufficient statistics on such cage sizes by experimentally forming numerous large grains at each dimer concentration ϕ_d, this is not feasible within a reasonable time frame. Instead, we numerically simulate ensembles of large triangular crystal grains containing 10^4 to 1.6×10^5 lattice sites for each value of ϕ_d.

Each simulated mixed crystal is initialized as a perfect triangular lattice of unbonded sites with periodic boundary conditions. In order to achieve the desired dimer concentration ϕ_d, bonds are added at random between neighboring lattice sites, creating dimers on the lattice. An example of such a numerically calculated mixed crystal with ϕ_d=0.3 is shown in Fig. 2(a) (for clarity, only a subset of the 10^4 lattice sites is shown). The distribution of dimer orientations, shown in Fig. 2(b), demonstrates that the three lattice directions are equally populated.

III. SCALING OF DISLOCATION CAGE SIZES WITH DIMER CONCENTRATION

The distribution of dislocation cage sizes z, taken over an ensemble of large mixed crystals for each dimer concentration, is plotted for $\phi_d=\{0.1,0.2,\ldots,1.0\}$ in Fig. 3. At least 10^5 individual cage sizes are included in the distributions for each dimer concentration, and the error bars due to counting statistics are comparable to the marker size. For clarity, the inset of Fig. 3 shows the same distributions on a semilogarithmic plot. We find that a functional form of $\rho(z)=Aze^{-z/z_*}$ fits the cage size distributions observed for every dimer concentration. While this fit was empirically determined here, we note that the functional form is consistent with exponentially decaying orientation correlations for dimers on a triangular lattice [20]. Although the fit is not perfect for small cage sizes z, it does accurately determine the peak cage size z_* for each dimer concentration.

We find that the peak cage size z_* taken from the fit for each distribution decreases smoothly with ϕ_d, as shown in Fig. 4. The line is the best-fit power law $z_*=Z_0\phi_d^{-\alpha}$, with $Z_0=6.3\pm0.1$ LC and $\alpha=0.98\pm0.02$. We note that the value of the peak cage size for a crystal of pure dimers is consistent with the previously reported average maximum glide distance of 6.2 LC [14]. This scaling of cage size with dimer concentration can be understood by noting that a cage is simply a row of lattice sites bounded by two parallel dimers in the blocking orientation. We can describe z_* as the average separation between such parallel dimers—that is, for every z_*

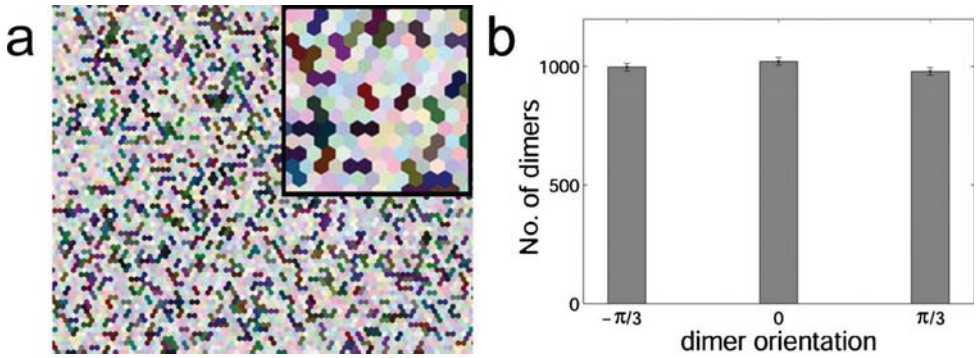

FIG. 2. (Color online) Example of a numerically calculated mixed crystal with dimer concentration ϕ_d=0.3. (a) The lattice sites that are dimer bonded are shaded in matching darker hues, while the sphere lattice sites are uniquely shaded lighter hues. Inset: zoomed-in view illustrating the shade coding for dimers versus spheres. (b) The distribution of dimer orientations for this mixed crystal demonstrates that the three lattice directions are equally weighted. Error bars are derived from counting statistics.

lattice sites on a crystalline row, there must be one dimer in the blocking orientation. Since the probability of encountering any dimer lobe on a lattice site is ϕ_d, and since each dimer can be oriented in any of six directions, we would expect that $1/z_* = \phi_d/6$. This prediction is plotted as a dotted line in Fig. 4. Note that this prediction assumes that there are no correlations between dimer orientations, an assumption that is best for small ϕ_d where dimers are separated by larger distances so that their orientations are no longer correlated. Indeed, Fig. 4 indicates that the agreement between this prediction and the simulation data is strongest for lower ϕ_d.

IV. VACANCY-MEDIATED UNCAGING AND VACANCY DIFFUSION

The distributions of cage sizes in the simulated mixed crystals suggest that the transition into restricted dislocation motion is characterized by smoothly decreasing dislocation cage sizes. At zero dimer concentration, cages are infinitely large, indicating that dislocation glide is completely unrestricted. Interestingly, the addition of any nonzero fraction of dimers ϕ_d immediately introduces finite cage sizes, so that in an infinitely large crystal, any dislocation is caged. This result is surprising because it suggests that there is some degree of dislocation glassiness in the system even for very small concentrations of dimers.

In pure dimer crystals, slow multidefect mechanisms involving collaboration between multiple dislocations is required to uncage a dislocation [14]. However, we observe another uncaging mechanism in experimental mixed crystals with low dimer concentrations ϕ_d. Figure 5 depicts a dislocation uncaging event that does not require the collaboration of multiple dislocations. In Fig. 5(a), a dislocation glides along a crystalline axis until it encounters a dimer in a blocking orientation along its path. While in crystals of pure dimers such an obstruction would prevent the dislocation from continuing any further, in this low ϕ_d mixed crystal, the dislocation circumvents the blocking particle by climbing 1 LC to the next row [Fig. 5(b)]. Dislocation climb is more energetically expensive than dislocation glide, and this

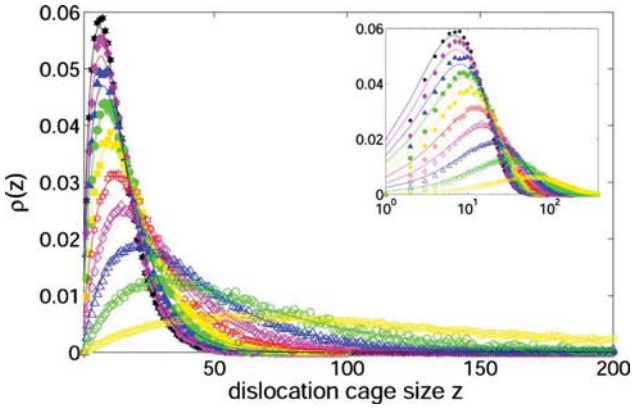

FIG. 3. (Color online) The distribution of cage sizes from numerically simulated mixed crystals for each dimer concentration. Marker key—from top curve to bottom curve: ϕ_d=1.0 (solid black stars), 0.9 (solid purple diamonds), 0.8 (solid blue triangles), 0.7 (solid green circles), 0.6 (solid yellow squares), 0.5 (open red stars), 0.4 (open purple diamonds), 0.3 (open blue triangles), 0.2 (open green circles), and 0.1 (open yellow squares). The curves are fits as described in the text. The distribution is also shown in a semilogarithmic plot as the inset.

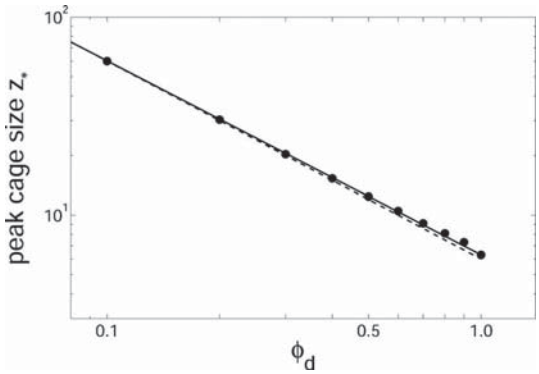

FIG. 4. The peak cage size z_* as a function of dimer concentration ϕ_d. The solid line is the best-fit power law, as described in the text. The dotted line is the theoretical prediction $z_*=6/\phi_d$, which ignores correlations between dimer orientations. Error bars derived from counting statistics are comparable to the marker size.

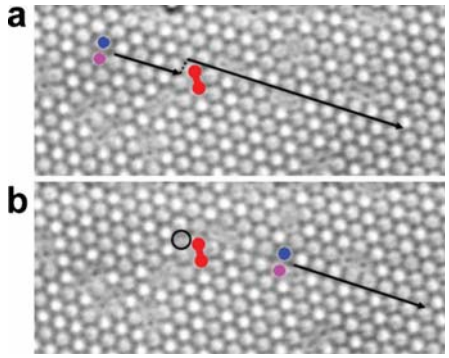

FIG. 5. (Color online) Time series micrographs of a climb event in a very low dimer concentration mixed crystal. (a) A dislocation gliding along a crystal plane is blocked by the dimer highlighted in red (grey). (b) When the dislocation reaches the caging dimer, it produces a vacancy (highlighted with a black circle) and climbs by one lattice constant, thereby escaping the cage and continuing to glide unobstructed.

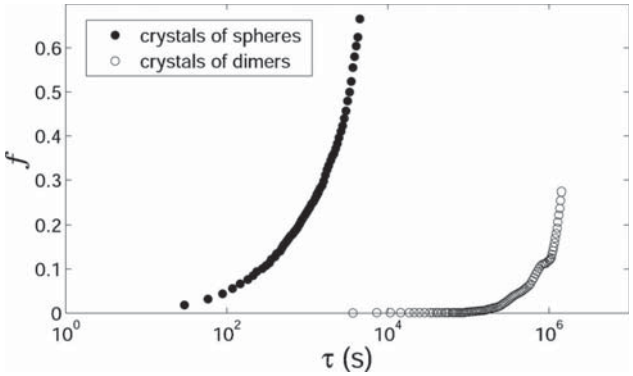

FIG. 6. The fraction f of vacancies that have completed at least one lattice hop within a waiting time τ is plotted for both experimental crystals of pure dimers (open circles) and experimental crystals of pure spheres (closed circles). Error bars derived from counting statistics are comparable to the marker size. The clear separation between the two curves indicates that the hopping time is slower by a factor of approximately 3 orders of magnitude in crystals of dimers compared to crystals of spheres.

mechanism typically involves either the emission or absorption of a vacancy. The vacancy emitted during the climb event shown in Fig. 5 is highlighted with a circle in Fig. 5(b).

In order for the vacancy-mediated uncaging mechanism to function in an equilibrated crystal, balance must be maintained between vacancy creation and vacancy loss. This balance requires that any vacancies produced during a climb event must eventually leave the crystal, either by diffusing to the grain boundary or by being absorbed during another climb event. In order for such vacancy elimination to occur, the vacancies must be free to move throughout the crystal on the time scale of dislocation motion. While in principle climb mechanisms involving vacancies could also occur in degenerate crystals of pure dimers, such events have not been experimentally observed [14,18]. In fact, experiments indicate that vacancies in pure dimer crystals rarely move from their initial lattice positions.

While it is difficult to experimentally isolate differences in vacancy diffusion between crystals of pure spheres and pure dimers, a rough estimate of vacancy hopping times in two similarly prepared crystals can provide valuable intuition. To this end, we prepare crystals in wedge cells tilted at the same angle, so that the lobe area fraction in both the sphere crystals and the dimer crystals is ~0.8. We find that vacancies diffuse dramatically more slowly in dimer crystals. The fraction f of vacancies that hop at least one lattice site within a waiting time τ is plotted for both crystals of dimers and crystals of spheres in Fig. 6. The data indicate that vacancies in dimer crystals take approximately 10^3 times longer to hop from one site to the next, suggesting that restrictions on vacancy hops caused by dimer particles can have a dramatic effect on the resulting vacancy diffusion.

Figures 7(a) and 7(b) depict the only mechanism for vacancy diffusion that we have observed within experimental pure dimer crystal grains. A vacancy hops from one lattice site to a neighboring lattice site via the swinging motion of a neighboring dimer. In principle, "sliding" moves, depicted schematically by the motion of the dimer highlighted in Fig. 7(c), could also allow a vacancy hop. However, such moves have not been experimentally observed within crystal grains, probably because they are more energetically costly, as suggested by the overlap volumes depicted in yellow in Fig. 7(c). Since only certain dimer orientations allow vacancies to hop, we expect that vacancy diffusion is dramatically slower in dimer crystals.

In order to isolate this phenomenon and study how this slowed vacancy diffusion scales with dimer concentration, we perform numerical Monte Carlo simulations of vacancy motion on a lattice in mixed crystals with increasing concentrations of dimers. In these simulations at each time step, a vacancy hop is attempted from the vacancy's current lattice site to any one of its six nearest-neighbor sites with equal probability. The vacancy hop to that site is allowed if the potential site is either occupied by a sphere or by a dimer lobe that can swing into the current vacancy site. The hop is not allowed if the potential site is occupied by a dimer lobe that cannot swing into the current vacancy site. Vacancy diffusion on the lattice according to these vacancy hop rules is

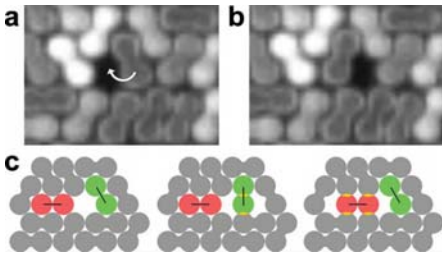

FIG. 7. (Color online) Mechanisms for vacancy diffusion in pure dimer crystals. (a) and (b) In an experimental dimer crystal, a vacancy hops one lattice site via the swinging motion of a neighboring dimer. This is the only vacancy hop mechanism that has been observed in the experiments. (c) A cartoon depiction of the maximal overlap area during a simplified model of a dimer swinging move and a dimer sliding move. The total overlap area required for a sliding move is twice that for a swinging move.

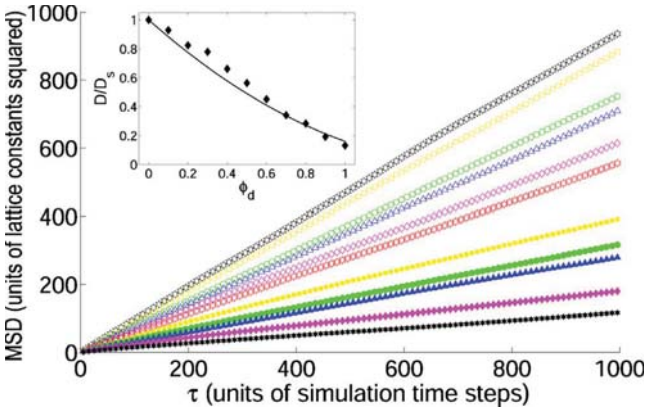

FIG. 8. (Color online) Vacancy mean-squared displacement in simulated mixed crystals of dimers and spheres. Marker key—from bottom curve to top curve: $\phi_d=1.0$ (solid black stars), 0.9 (solid purple diamonds), 0.8 (solid blue triangles), 0.7 (solid green circles), 0.6 (solid yellow squares), 0.5 (open red stars), 0.4 (open purple diamonds), 0.3 (open blue triangles), 0.2 (open green circles), 0.1 (open yellow squares), and 0.0 (open black stars). Inset: the best-fit scaled diffusion constant D/D_s over the range $\tau=1-10^3$ simulation time steps is plotted as a function of dimer fraction ϕ_d. The solid curve is the theoretical prediction $D/D_s=[1-(3/5)\phi_d]^2$.

recorded for mixed crystals containing 10^4 lattice sites for each dimer concentration $\phi_d=\{0,0.2,0.4,\ldots,1.0\}$.

The vacancy mean-squared displacement (MSD)$=\langle\Delta r^2\rangle$ for each dimer concentration is plotted in Fig. 8. Each MSD data series is determined from over 10^5 vacancy hop attempts, and the error bars due to counting statistics are on the order of the marker size. The diffusion constant for vacancies in pure sphere crystals ($\phi_d=0$), determined from the best-fit curve of the form MSD$=\langle\Delta r^2\rangle=4D\tau$, is found to be $D_s=0.235\pm0.001$ LC^2 per time step. As the dimer concentration increases, the diffusion constant decreases, reaching 0.031 ± 0.001 LC^2 per time step for pure dimer crystals. The best-fit scaled diffusion constant D/D_s is calculated for each dimer concentration and is plotted in the inset of Fig. 8.

The functional form of the decay of the scaled diffusion constant with dimer concentration ϕ_d can be theoretically predicted in the limit that correlations between dimer orientations may be ignored. In this case, the probability that a vacancy in a given lattice site will *not* make a successful hop is the product of the probability that the site contains a dimer lobe and the probability that the dimer is in one of the three nonswinging orientations of its five possible orientations as depicted by the red dashed thicker lines in Fig. 9. Thus, the probability that the vacancy *can* successfully make the hop is $1-(3/5)\phi_d$. This hopping probability causes the average step size for vacancies diffusing in a mixed crystal to be smaller by a factor of $1-(3/5)\phi_d$ than the step size taken in a crystal of spheres over the same time interval. Since the vacancy diffusion constant scales as the square of the average step size, in a mixed crystal the diffusion constant would be $D=[1-(3/5)\phi_d]^2D_s$. This theoretical prediction is plotted as the solid curve in the inset of Fig. 9 and is consistent with the simulated data.

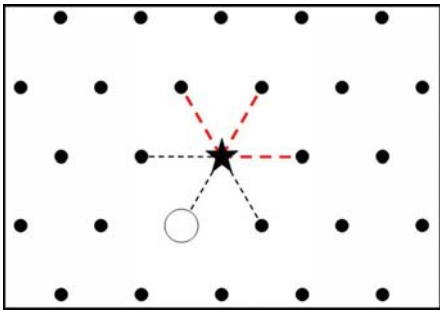

FIG. 9. (Color online) Schematic showing the possible dimer orientations with one dimer lobe in a potential vacancy site. The current vacancy site is marked with an open circle, and the potential vacancy site is marked with a star. Of the five possible dimer orientations shown with dashed lines, the three highlighted in red with thicker dashed lines do not allow dimer swinging.

V. DISCUSSION AND CONCLUSIONS

The transition from unrestricted dislocation motion in crystals of pure spheres to the glassy caged dislocation dynamics observed in crystals of pure dimers has been studied both experimentally and with numerical simulations of mixed crystals. We find that while cages restricting dislocation glide are present for mixed crystals with any nonzero dimer concentration ϕ_d, we also observe a vacancy-mediated uncaging mechanism. This mechanism can release dislocations from glide-restricted cages and has the potential to alleviate the glassy dynamics that arise from dislocation caging, ultimately driving the system out of the glassy state. Vacancy diffusion is sufficiently fast in crystals of spheres to maintain the balance between the rate of vacancy creation and loss necessary for maintaining equilibrium. The addition of a small fraction of dimers only reduces the vacancy diffusion by a factor of $[1-(3/5)\phi_d]^2$ for small ϕ_d. As the dimer concentration approaches 1, vacancy diffusion becomes prohibitively slow and suppresses such vacancy-mediated uncaging.

This study has fleshed out the details of both dislocation and vacancy mobility as dimers are added to crystals of spheres. Clearly the transition from the usual unrestricted dislocation dynamics in crystals of spheres into the glassy dynamics observed in pure dimers is complex and depends on additional dislocation transport mechanisms besides simple glide. Future experimental studies of the relaxation responses of mixed sphere and dimer crystals should help to elucidate whether this vacancy-mediated uncaging mechanism is actually sufficient to drive the system out of the glassy state. If so, such studies should determine whether there is a crossover dimer concentration beyond which vacancy mobility is low enough that the dislocation dynamics become glassy.

Our results illustrate the delicate interplay between dislocations and vacancies that arises in mixed crystals of dimers and spheres. We expect that these results will provide a framework for interpreting defect restrictions and interactions in crystals doped with dislocation constraining impurities and crystals comprised of other anisotropic particles

[21–28]. Finally, this work highlights the importance of geometrical constraints in determining not only individual defect dynamics but also their interactions within the crystal.

ACKNOWLEDGMENTS

We thank Jim Sethna, Stefano Zapperi, Fernando Escobedo, Umang Agarwal, Carl Franck, Stephanie Lee, Erin Riley, and the Cohen group for helpful discussions. This research was supported in part by the Department of Energy, Basic Energy Sciences, Grant No. ER46517 (fabrication of colloidal assemblies and manipulation with optical trap) and in part by Award No. KUS-C1-018-02 from King Abdullah University of Science and Technology (KAUST).

APPENDIX: METHODS—RAMP CELL CONSTRUCTION

The wedge-shaped confinement cells are constructed using a $2'' \times 3''$ microscope slide with two No. 1.5 (170-μm)-thick 20×55 mm^2 coverslips. One coverslip is bonded to the microscope slide using UV glue (Norland Adhesive) to provide a structural base for the confinement cell [Fig. 10(a)]. Both coverslips must be soaked for 30 min in a base wash solution of NaOH (pH$\approx$14) to remove the coating that is applied during manufacturing to prevent the coverslips from sticking together. The coverslips are then individually rinsed with DI H_2O and dried using forced filtered air.

After this washing procedure, the glass coverslips are clean enough that when pressure is applied, two coverslips will bond together. In order to achieve the wedge-shaped geometry, before the two coverslips are bonded together, small spacers are added to the coverslip on the slide by curing two rows of tiny droplets of UV glue as depicted in Fig. 10(b). After the spacers are cured, the second coverslip is placed on top of the first, and the two are squeezed together until a bond forms at the end without spacers [Fig. 10(c)]. UV glue is then used to seal three sides of the cell, leaving an access gap in the spacer end [Fig. 10(c)]. After a colloidal sample is pipetted in through the top access gap, UV glue is used to seal the cell. The region of the cell that only accommodates one layer of $\sim$1-μm-sized particles is typically found several mm above the edge of the bonded region. The slope of the wedge in the monolayer region is about 1 μm over 1 mm. Colloidal suspensions confined in such wedge-shaped cells can be stored for long time periods exceeding 2 years without any sample evaporation or degradation.

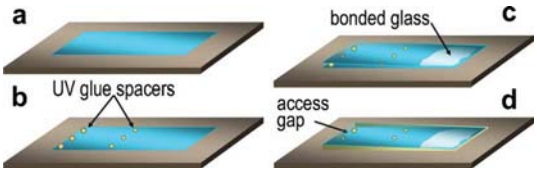

FIG. 10. (Color online) Schematic of wedge-shaped confinement cell construction. The wedge angle is exaggerated for clarity. (a) One base-washed coverslip (blue) is bonded with UV glue to a larger microscope slide (beige) to provide structural support for the cell. (b) Small UV glue droplets (yellow) are placed in two rows on the coverslip and are cured to become spacers for the cell. (c) A second base-washed coverslip is placed on top of the first, and the two are squeezed together until the two coverslips bond together (bonded region shown in white). (d) UV glue (shown in yellow) is then used to seal three sides of the cell, leaving an access gap for inserting colloidal samples. Once the cell is filled with sample, this gap is also sealed using UV glue.

[1] J. B. Knight, C. G. Fandrich, C. N. Lau, H. M. Jaeger, and S. R. Nagel, Phys. Rev. E **51**, 3957 (1995).
[2] J. Brujić, P. Wang, C. Song, D. L. Johnson, O. Sindt, and H. A. Makse, Phys. Rev. Lett. **95**, 128001 (2005).
[3] M. Mailman, C. F. Schreck, C. S. O'Hern, and B. Chakraborty, Phys. Rev. Lett. **102**, 255501 (2009).
[4] E. R. Weeks, J. C. Crocker, A. C. Levitt, A. Schofield, and D. A. Weitz, Science **287**, 627 (2000).
[5] E. R. Weeks and D. A. Weitz, Phys. Rev. Lett. **89**, 095704 (2002).
[6] K. Zhao and T. G. Mason, Phys. Rev. Lett. **103**, 208302 (2009).
[7] P. Yunker, Z. Zhang, and A. G. Yodh, Phys. Rev. Lett. **104**, 015701 (2010).
[8] M. Hermes and M. Dijkstra, EPL **89**, 38005 (2010).
[9] S. I. Simdyankin and N. Mousseau, Phys. Rev. E **68**, 041110 (2003).
[10] M. D. Ediger, C. A. Angell, and S. R. Nagel, J. Phys. Chem. **100**, 13200 (1996).
[11] G. Lois, J. Blawzdziewicz, and C. S. O'Hern, Phys. Rev. Lett. **102**, 015702 (2009).
[12] N. Xu, T. K. Haxton, A. J. Liu, and S. R. Nagel, Phys. Rev. Lett. **103**, 245701 (2009).
[13] D. Kivelson, W. Steffen, G. Meier, and A. Patkowski, J. Chem. Phys. **95**, 1943 (1991).
[14] S. J. Gerbode, U. Agarwal, D. C. Ong, C. M. Liddell, F. A. Escobedo, and I. Cohen, Phys. Rev. Lett. **105**, 078301 (2010).
[15] K. W. Wojciechowski, D. Frenkel, and A. C. Branka, Phys. Rev. Lett. **66**, 3168 (1991).
[16] K. W. Wojciechowski, Phys. Rev. B **46**, 26 (1992).
[17] S. H. Lee, S. J. Gerbode, B. S. John, A. K. Wolfgang, F. A. Escobedo, I. Cohen, and C. M. Liddell, J. Mater. Chem. **18**, 4912 (2008).
[18] S. J. Gerbode, S. H. Lee, C. M. Liddell, and I. Cohen, Phys. Rev. Lett. **101**, 058302 (2008).
[19] In crystals of spheres, the lobe area fraction is the particle area fraction. In crystals of dimers, the lobe area fraction is defined as the fraction of area occupied by the dimer lobes and does not include the area occupied by the waist.
[20] R. Moessner and S. L. Sondhi, Phys. Rev. Lett. **86**, 1881 (2001).
[21] J. Kim, R. J. Larsen, and D. A. Weitz, Adv. Mater. **19**, 2005 (2007).
[22] V. N. Manoharan, M. T. Elsesser, and D. J. Pine, Science **301**,

483 (2003).
[23] C. J. Hernandez and T. G. Mason, J. Phys. Chem. C **111**, 4477 (2007).
[24] S. C. Glotzer and M. J. Solomon, Nature Mater. **6**, 557 (2007).
[25] M. J. Solomon, R. Zeitoun, D. Ortiz, K. E. Sung, D. Deng, A. Shah, M. A. Burns, S. C. Glotzer, and J. M. Millunchick, Macromol. Rapid Commun. **31**, 196 (2010).
[26] Y.-S. Cho, G.-R. Yi, S.-H. Kim, S.-J. Jeon, M. T. Elsesser, H. K. Yu, S.-M. Yang, and D. J. Pine, Chem. Mater. **19**, 3183 (2007).
[27] C. J. Olson, C. Reichhardt, M. McCloskey, and R. J. Zieve, EPL **57**, 904 (2002).
[28] J.-G. Park, J. Forster, and E. R. Dufresne, J. Am. Chem. Soc. **132**, 5960 (2010).